Molecular Electronics

International Edition: DOI: 10.1002/anie.201603961
German Edition: DOI: 10.1002/ange.201603961

Observation of Charge Separation and Space-Charge Region in Single-Crystal P3HT/C_{60} Heterojunction Nanowires

*Kyung Sun Park, Ki Seok Lee, Jangmi Baek, Lynn Lee, Byung Hee Son, Yong-Eun Koo Lee, Yeong Hwan Ahn, Won Il Park, Youngjong Kang, and Myung M. Sung**

Abstract: *We directly observed charge separation and a space-charge region in an organic single-crystal p–n heterojunction nanowire, by means of scanning photocurrent microscopy. The axial p–n heterojunction nanowire had a well-defined planar junction, consisted of P3HT (p-type) and C_{60} (n-type) single crystals and was fabricated by means of the recently developed inkjet-assisted nanotransfer printing technique. The depletion region formed at the p–n junction was directly observed by exploring the spatial distribution of photogenerated carriers along the heterojunction nanowire under various applied bias voltages. Our study provides a facile approach toward the precise characterization of charge transport in organic heterojunction systems as well as the design of efficient nanoscale organic optoelectronic devices.*

Organic p–n junctions are essential components for the operation and performance of organic optoelectronic devices, such as organic photovoltaics, optical displays, organic light emitting diodes, organic transistors, and sensors.[1,2] Particularly, control over the charge transport processes at the junction regions has been a key strategy to achieve significant improvements in the performance of organic optoelectronic devices.[3–6] For instance, carrier transport efficiency can be increased by controlling charge injection and transport properties as well as charge-separation processes in organic/metal and organic/organic heterojunctions.[7,8] The charge transport across the heterojunctions has been explained by a flat band structure, or energy-level bending over a space-charge region.[8,9] The elucidation of the electronic structures at the junctions forms the basis for understanding and improving the performance of the organic optoelectronic devices. Despite the importance of this issue, there have been only a few measurements of interfacial energy structures and space-charge regions in organic heterojunctions by means of ultraviolet photoelectron spectroscopy (UPS) and scanning Kelvin probe microscopy (SKPM).[3,4,10–15] Moreover, these measurements were made mostly using organic bulk heterojunctions (BHJs) that contained randomly distributed junctions, and thus represent average transport properties of the bulk that contains many complicated interfacial networks. Also, most of these studies were conducted on amorphous or poorly crystalline materials, so the measured values may not represent the material's intrinsic properties.

Use of single-crystal material having a precisely defined interface is a prerequisite for the reliable measurement of the properties of charge transport over the junction. In particular, the one-dimensional single-crystal structure is the most suitable form for studying charge transport processes because of its perfect molecular order, absence of grain boundaries, good contact interfaces, and minimal number of charge traps.[16] It allows charge carriers to move only in one direction, enabling the intrinsic material properties to be determined. Regarding single-crystal inorganic heterojunction nanowires, there have been many studies in which the carrier transport behaviors have been observed and the diffusion lengths have been measured directly by using several techniques: time-resolved scanning photocurrent microscopy (SPCM),[17–19] SPCM combined with near-field scanning optical microscopy (NSOM),[20] a combination of atomic force microscopy (AFM) and NSOM,[21] and electron beam-induced current (EBIC).[22] These methods allow mapping of photogenerated carriers by means of monitoring local currents while a focused laser beam is scanned over an area of interest. However, no such measurements have been reported for single-crystal organic heterojunction nanowires, probably owing to the difficulties of fabricating these materials with a precisely defined interface.

Herein we fabricated an organic axial p–n heterojunction nanowire containing p-type and n-type organic single-crystal semiconductors and having a well-defined planar junction, by means of a recently developed inkjet-assisted nanotransfer printing (inkjet-NTP) technique.[23] Poly(3-hexylthiophene-2,5-diyl) (P3HT) and fullerene (C_{60}) are used as the p-type and n-type semiconducting materials, respectively. The resulting P3HT/C_{60} heterojunction nanowire devices were amenable to scanning photocurrent microscopy (SPCM) analysis, which allowed observation of apparent charge separation at the p–n junction and measurements of depletion width under various bias voltages. To our knowledge, this is the first direct observation of charge separation and depletion region formation in single-crystal organic p–n junctions.

For direct measurement of charge carrier transport properties in an organic heterojunction system, a precisely

[*] Dr. K. S. Park, K. S. Lee, J. Baek, L. Lee, Dr. Y. Koo Lee, Prof. Y. Kang, Prof. M. M. Sung
Department of Chemistry
Hanyang University
Seoul, 04763 (South Korea)
E-mail: smm@hanyang.ac.kr
B. H. Son, Prof. Y. H. Ahn
Department of Physics, Ajou University
Suwon, 16499 (South Korea)
Prof. W. I. Park
Department of Materials Science and Engineering
Hanyang University
Seoul, 04763 (South Korea)

Supporting information for this article can be found under: http://dx.doi.org/10.1002/anie.201603961.

defined junction between two organic crystals should be realized. Figure 1 schematically illustrates the fabrication of an axial p–n heterojunction based on P3HT and C_{60} crystalline nanowires by means of the simple Inkjet-NTP process.[23] First, a pattern of nanoscale lines is fabricated on a silicon wafer by means of e-beam lithography; each line is 100 nm wide and 200 nm tall, and adjacent lines are spaced 3 μm apart. A negative mold of these lines is fabricated by casting polyurethane acrylate (PUA) onto the pattern. Second, a droplet of P3HT ink solution is applied to the PUA mold, filling only the engraved channels owing to capillary force. The P3HT ink solution inside the nanoscale channel of the mold is solidified by drying at a mild temperature (< 70 °C), resulting in a single-crystal P3HT nanowire by means of self-assembly and crystallization of P3HT molecules.[24,25] Third, C_{60} nanowires are fabricated adjacent to the P3HT nanowires by means of the same procedure, thereby forming p–n heterojunction nanowires in the channels. Note that the P3HT nanowire should be completely dried before deposition of the C_{60} ink solution so as to avoid blending of the two inks. Also, the C_{60} ink solution is prepared in tetralin solvent, in which P3HT is nearly insoluble; this ensures a clearly defined planar junction at the P3HT/C_{60} interface. Fourth, the mold containing the heterojunction nanowires is contacted with a substrate. Between the mold and the substrate, a thin layer of a polar solvent is applied so as to allow good conformal contact between the elastomeric mold containing the P3HT/C_{60} nanowires and the substrate.[24] The solvent should be carefully selected to dissolve neither the P3HT nanowires nor the C_{60} nanowires. The solvent layer is then evaporated by means of a drying process, which pulls the P3HT/C_{60} nanowires down from the mold to the substrate, resulting in axial p–n heterojunction nanowires each having a well-defined planar junction.

Several different imaging techniques were used for characterization of the P3HT/C_{60} heterojunction nanowires. Scanning electron microscopy (SEM) of a P3HT/C_{60} heterojunction nanowire revealed a clearly defined planar interface between the two different materials (Figure 2a). The nanowire was about 100 nm in diameter and had a smooth surface. The heterojunction structure was also confirmed by dark-field

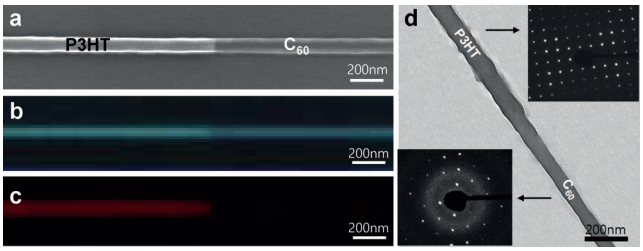

Figure 2. a) SEM, b) DF-OM, and c) PL-OM images of a P3HT/C_{60} heterojunction nanowire. d) TEM image of the heterojunction nanowire. Insets: SAED patterns of the nanowire segments P3HT (top right), C_{60} (bottom left).

optical microscopy (DF-OM) and photoluminescence optical microscopy (PL-OM). The DF-OM image of the heterojunction nanowire (Figure 2b) shows distinct color contrast between the two materials owing to their different refractive indices.[26,27] In the PL-OM image (Figure 2c), the bright red part of the single p–n junction nanowire is attributed to P3HT; specifically, its surface-trap emission is at around 645–700 nm excited by 495–570 nm light.[28] The dark part is attributed to C_{60} that rarely exhibits photoluminescence under such excitation. Structural analysis of the heterojunction nanowire was carried out by means of transmission electron microscopy (TEM) and selected-area electron diffraction (SAED). Figure 2d shows a TEM image of the heterojunction nanowire and corresponding SAED patterns of its P3HT and C_{60} segment. The TEM image clearly shows the distinct morphology difference between the materials and the formation of an interface between them; the SAED patterns indicate that both components have single-crystal structures. For the analysis of the crystal structure, lattice unit cell modeling and corresponding electron diffraction simulations were carried out.[29] The SAED pattern of the P3HT segment was identified as the (100) plane of an orthorhombic crystal. The C_{60} pattern showed reflections of a face centered cubic (fcc) structure oriented along the [111] zone axis. These observations are in good agreement with previous reports on nanoscale P3HT and C_{60} single crystals.[24] Overall, these results indicate that the heterojunction nanowire was com-

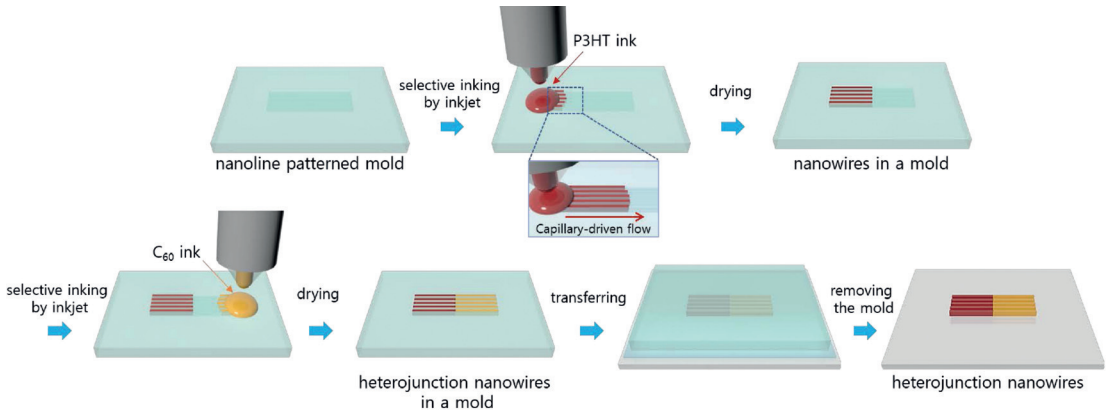

Figure 1. Schematic illustration of the procedure used to fabricate organic axial p–n heterojunction nanowires by means of inkjet-NTP. First, single-crystal P3HT nanowires (red) are synthesized and crystallized in molded nanoscale channels. Then, C_{60} nanowires (orange) are similarly prepared adjacent to the P3HT nanowires, forming p–n heterojunction nanowires and these are printed onto a substrate.

posed of single-crystalline P3HT and C_{60} and had a well-defined planar interface between them.

For electrical characterization, a single-crystal axial P3HT/C_{60} heterojunction nanowire device was fabricated as shown in Figure 3a. First, the single-crystal P3HT/C_{60} heterojunction nanowires, as the active channel layers, were printed on the substrate by means of inkjet-NTP as detailed above. Subsequently, to contact the nanowires, Au source and drain electrodes separated by a distance of 60 μm were defined by means of thermal evaporation. The DF-OM image in Figure 3b clearly shows 20 of the heterojunction nanowires (each 100 nm wide and spaced 3 μm apart). The PL-OM image in Figure 3b shows that each heterojunction nanowire (P3HT on the left and C_{60} on the right) has a well-defined junction between the Au electrodes. The P3HT/C_{60} heterojunction nanowire device exhibited rectifying behaviors, typical current–voltage (*I–V*) characteristics of a diode (Figure 3c). In a p–n junction, rectification arises from the potential barrier formed at the interface between the p-type and n-type semiconductor materials. In the *I–V* curve (Figure 3c), under forward bias the current increases with the bias voltage owing to decrease of the potential barrier, whereas under reverse bias only a small amount of current flows because the barrier height increases with the bias voltage. The rectification ratio, defined as the ratio of forward to backward current measured at the same absolute bias, is about 25 at 50 V (Figure 3c, inset). Figure 3d shows the photo-response of the P3HT/C_{60} heterojunction nanowire device. Under illumination, both the forward and reverse currents increased because of the generation of charge carriers on the nanowires. The photo gain, defined as the photocurrent divided by the dark current, was 4.4 at 50 V under the light intensity of 12.2 mW cm^{-2}. Note that we applied external electrical field to observe the photo-response behaviors because the electric field induced by the built-in potential was too small to produce a detectable amount of charge carriers owing to the small junction area (ca. 2×10^{-10} cm^2) and the relatively high nanowire length.

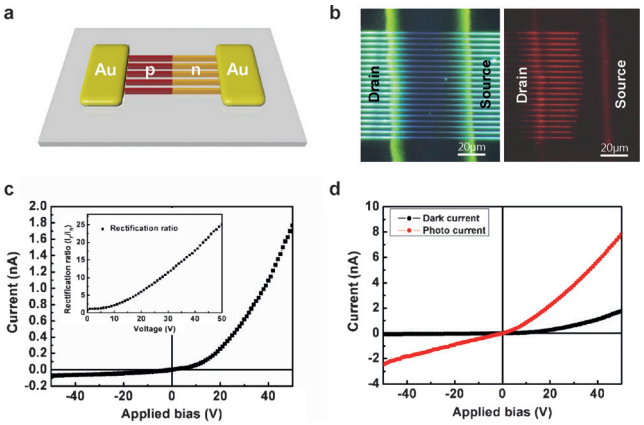

Figure 3. a) Schematic representation of an axial p–n heterojunction nanowire device. b) DF-OM and PL-OM images of 20 P3HT/C_{60} heterojunction nanowires with metal contacts. c) *I–V* characteristics of the P3HT/C60 heterojunction nanowire device; inset: a plot of the device rectification ratio versus voltage. d) *I–V* characteristics of the P3HT/C_{60} heterojunction device in the dark (black) and under 12.2 mW cm^{-2} illumination (red).

SPCM is widely used for monitoring the carrier dynamics near the interfaces of heterojunctions to investigate the processes of carrier diffusion and drift (driven by a built-in potential and external potential).[30,31] Through spatial distribution analysis of the locally excited photocarriers using SPCM, we were able to observe the donor/acceptor interface and to determine the depletion width in the single-crystal P3HT/C_{60} heterojunction nanowires. The SPCM measurement setup is illustrated schematically in Figure 4a. In the SPCM measurements, a focused laser ($\lambda = 532$ nm) was scanned along each heterojunction nanowire in the device using a two-axis galvo scanner, creating localized carriers that gave rise to a current, that is, a photocurrent. The photocurrent was collected using a lock-in amplifier synched at the modulation frequency of the incident laser. The photocurrent was measured at a series of reverse bias voltages from 0 to −60 V, with 10 V increments. In a representative photocurrent microscopic image from SPCM measurements on the heterojunction nanowire device taken at $V_b = -40$ V, strong photocurrent peaks were observed in the middle, junction regions of the heterojunction nanowires (Figure 4b); this indicates that the photoexcited carriers were effectively separated at the junction and collected in the form of photocurrent.[32–34] A maximum photocurrent was only observed at the junction region of each nanowire, indicating that each had a well-defined planar junction.

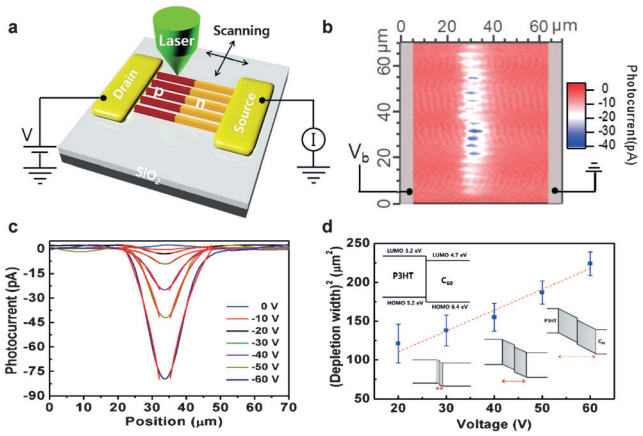

Figure 4. a) Schematic illustration of the SPCM measurement setup. A laser is scanned along the p–n junction nanowires in the organic heterojunction nanowire device and photocurrent measurements are collected as a function of applied bias voltage. b) SPCM image of the heterojunction nanowire device, collected at $V_b = -40$ V; gray bars indicate the metal contacts. c) Photocurrent versus position along the nanowire for bias voltages ranging from 0 to −60 V; red lines indicate exponential fitting curves used to extract depletion widths. d) Squares of measured depletion widths (blue dots with error bars) versus bias voltage; the red dotted line is a linear fit. Insets: top left) the energy level diagram of the two nanowire materials and bottom right) diagrams of the change in depletion width (red dotted line with arrows) with applied bias voltage.

Figure 4c shows representative line profiles of photocurrent versus position along the nanowire axis at various applied bias voltages (V_b of 0 to −60 V). As the bias voltage was increased, the photocurrent peak heights increased. Note that no significant photocurrent was observed for low bias voltages (0 to −10 V), probably owing to the small junction area and the relatively long channel length (60 μm) used in our devices. The increase in photocurrent at higher bias voltages mainly arose from more effective separation and collection of photoexcited carriers under conditions of higher electric field. Under the high bias voltages, carrier diffusion is negligible because carrier transport at the junction is mainly influenced by drift rather than diffusion under a strong external electric field.[35,36] The photocurrent profiles for high bias voltages (−20 to −60 V) from the peak near the p–n junction can be used to quantify the depletion width by fitting the exponential decay of the photocurrent to the equation $J \propto \exp(\pm(x-d)/L_{e,h})$, where d is the peak position and the plus and minus signs correspond to electrons and holes, respectively.[33] The decay lengths of electrons (L_e) and holes (L_h) were obtained by fitting the data in Figure 4c to this equation, yielding: L_e of 5.50, 5.72, 6.06, 6.98, and 7.32 μm, and; L_h of 4.48, 6.03, 6.42, 6.72, and 7.65 μm for V_b of −20, −30, −40, −50, and −60 V respectively. The total decay length ($L_e + L_h$) of electron and hole carriers, corresponding to the depletion width, was obtained for each bias voltage. The depletion widths from ten different devices (200 nanowires) were measured and averaged to yield the depletion widths plotted in Figure 4d. The depletion width (w) in a p–n junction can be estimated from the following relationship with external reverse bias voltage (V): $w = \sqrt{((2\varepsilon_0\varepsilon)/q\ (1/N_A + 1/N_D)(V_{bi} + V))}$, where V_{bi} is the built-in potential in the p–n junction; ε_0 is the vacuum permittivity; ε is the permittivity of the semiconductor; and N_A and N_D are carrier concentrations of the acceptor and donor materials, respectively. As demonstrated in Figure 4d, the squares of the measured depletion widths (blue dots with error bars) were linear with the bias voltage, showing a good fit to the above relationship (red line). The observed increase of depletion width with bias voltage probably resulted from a typical p–n junction device characteristic: the electric field at the junction is induced by the bias voltage (Figure 4d, inset). The single-crystal organic p–n heterojunction nanowire device measured in this study allows more precise characterization of the properties of the heterojunction materials, thus significantly reducing the uncertainty in data interpretation in comparison with that arising from the testing of bulk polycrystalline devices.

In summary, we have demonstrated that a single-crystal organic axial p–n heterojunction nanowire serves as a simple model system for understanding the fundamental charge transport at nanoscale donor/acceptor interfaces. Single-crystal axial P3HT/C_{60} heterojunction nanowires each having a well-defined junction region were fabricated by means of inkjet-NTP and were exploited for direct observation, by means of SPCM, of charge separation and depletion width in the junction region under external electric fields. Our study suggests the possibility of extending this approach to the study of charge transport in other organic heterojunctions, as well as to production of highly integrated organic optoelectronic devices.

Acknowledgements

This work was supported by National Research Foundation of Korea (NRF funded by the Ministry of Science, ICT & Future Planning) through the Global Frontier R&D Program on the Center for Multiscale Energy System (2012M3A6A7054855), by the Nano·Material Technology Development Program (2012M3A7B4034985), and by Creative Materials Discovery Program (2015M3D1A1068061). This work was also supported by a grant from the National Research Foundation of Korea (NRF), funded by the Korea government (MIST) (No. 2014R1A2A1A10050257), and by the Samsung Research Funding Center of Samsung Electronics under Project Number SRFC-MA1401-05.

Keywords: nanotransfer printing · optoelectronics · organic nanowires · p–n heterojunctions · space-charge region

How to cite: *Angew. Chem. Int. Ed.* **2016**, *55*, 10273–10277
Angew. Chem. **2016**, *128*, 10429–10433

[1] B. Kippelen, J. L. Bredas, *Energy Environ. Sci.* **2009**, *2*, 251–261.
[2] H. B. Wang, D. H. Yan, *NPG Asia Mater.* **2010**, *2*, 69–78.
[3] O. V. Molodtsova, T. Schwieger, M. Knupfer, *Appl. Surf. Sci.* **2005**, *252*, 143–147.
[4] Y. L. Gao, H. J. Ding, H. B. Wang, D. H. Yan, *Appl. Phys. Lett.* **2007**, *91*, 142112.
[5] F. Zhang, A. Vollmer, J. Zhang, Z. Xu, J. P. Rabe, N. Koch, *Org. Electron.* **2007**, *8*, 606–614.
[6] J. G. Tait, U. W. Paetzold, D. Cheyns, M. Turbiez, P. Heremans, B. P. Rand, *ACS Appl. Mater. Interfaces* **2016**, *8*, 2211–2219.
[7] S. Braun, W. R. Salaneck, M. Fahlman, *Adv. Mater.* **2009**, *21*, 1450–1472.
[8] H. Ishii, K. Sugiyama, E. Ito, K. Seki, *Adv. Mater.* **1999**, *11*, 972–972.
[9] F. Bussolotti, J. P. Yang, A. Hinderhofer, Y. L. Huang, W. Chen, S. Kera, A. T. S. Wee, N. Ueno, *Phys. Rev. B* **2014**, *89*, 115319.
[10] T. W. Ng, M. F. Lo, S. T. Lee, C. S. Lee, *Appl. Phys. Lett.* **2012**, *100*, 113301.
[11] P. Matyba, K. Maturova, M. Kemerink, N. D. Robinson, L. Edman, *Nat. Mater.* **2009**, *8*, 672–676.
[12] H. Ishii, N. Hayashi, E. Ito, Y. Washizu, K. Sugi, Y. Kimura, M. Niwano, Y. Ouchi, K. Seki, *Phys. Status Solidi A* **2004**, *201*, 1075–1094.
[13] T. W. Zeng, F. C. Hsu, Y. C. Tu, T. H. Lin, W. F. Su, *Chem. Phys. Lett.* **2009**, *479*, 105–108.
[14] H. Hoppe, T. Glatzel, M. Niggemann, A. Hinsch, M. C. Lux-Steiner, N. S. Sariciftci, *Nano Lett.* **2005**, *5*, 269–274.
[15] H. Y. Mao, F. Bussolotti, D. C. Qi, R. Wang, S. Kera, N. Ueno, A. T. S. Wee, W. Chen, *Org. Electron.* **2011**, *12*, 534–540.
[16] A. L. Briseno, S. C. B. Mannsfeld, S. A. Jenekhe, Z. Bao, Y. N. Xia, *Mater. Today* **2008**, *11*, 38–47.
[17] Y. Gu, J. P. Romankiewicz, J. K. David, J. L. Lensch, L. J. Lauhon, *Nano Lett.* **2006**, *6*, 948–952.
[18] M. D. Kelzenberg, D. B. Turner-Evans, B. M. Kayes, M. A. Filler, M. C. Putnam, N. S. Lewis, H. A. Atwater, *Nano Lett.* **2008**, *8*, 710–714.
[19] A. D. Mohite, D. E. Perea, S. Singh, S. A. Dayeh, I. H. Campbell, S. T. Picraux, H. Htoon, *Nano Lett.* **2012**, *12*, 1965–1971.

[20] Y. P. Dan, K. Seo, K. Takei, J. H. Meza, A. Javey, K. B. Crozier, *Nano Lett.* **2011**, *11*, 2527 – 2532.
[21] L. Baird, C. P. Ong, R. A. Cole, N. M. Haegel, A. A. Talin, Q. M. Li, G. T. Wang, *Appl. Phys. Lett.* **2011**, *98*, 132104.
[22] C. Gutsche, R. Niepelt, M. Gnauck, A. Lysov, W. Prost, C. Ronning, F. J. Tegude, *Nano Lett.* **2012**, *12*, 1453 – 1458.
[23] K. S. Park, J. Baek, Y. Park, L. Lee, Y. E. K. Lee, Y. Kang, M. M. Sung, *Adv. Mater.* **2016**, *28*, 2874 – 2880.
[24] K. S. Park, B. Cho, J. Baek, J. K. Hwang, H. Lee, M. M. Sung, *Adv. Funct. Mater.* **2013**, *23*, 4776 – 4784.
[25] G. Giri, S. Park, M. Vosgueritchian, M. M. Shulaker, Z. Bao, *Adv. Mater.* **2014**, *26*, 487 – 493.
[26] S. Y. Chuang, H. L. Chen, W. H. Lee, Y. C. Huang, W. F. Su, W. M. Jen, C. W. Chen, *J. Mater. Chem.* **2009**, *19*, 5554 – 5560.
[27] Z. B. Wang, M. G. Helander, J. Qiu, D. Gao, Y. L. Chang, Z. H. Lu, *Nanotechnology* **2012**, *23*, 344010.
[28] S. H. Lee, D. H. Park, K. Kim, J. Joo, D. C. Kim, H. J. Kim, J. Kim, *Appl. Phys. Lett.* **2007**, *91*, 263102.
[29] Commercial software packages (Single Crystal 2.2.5. Crystal Maker Software Ltd.) is used for data analysis.
[30] J. K. Park, J. C. Kang, S. Y. Kim, B. H. Son, J. Y. Park, S. Lee, Y. H. Ahn, *J. Phys. Chem. Lett.* **2012**, *3*, 3632 – 3638.
[31] J. D. Park, B. H. Son, J. K. Park, S. Y. Kim, J. Y. Park, S. Lee, Y. H. Ahn, *AIP Adv.* **2014**, *4*, 067106.
[32] Y. Gu, E. S. Kwak, J. L. Lensch, J. E. Allen, T. W. Odom, L. J. Lauhon, *Appl. Phys. Lett.* **2005**, *87*, 043111.
[33] T. Otto, C. Miller, J. Tolentino, Y. Liu, M. Law, D. Yu, *Nano Lett.* **2013**, *13*, 3463 – 3469.
[34] C. J. Lombardo, M. S. Glaz, Z. E. Ooi, D. A. Vanden Bout, A. Dodabalapur, *Phys. Chem. Chem. Phys.* **2012**, *14*, 13199 – 13203.
[35] R. Graham, C. Miller, E. Oh, D. Yu, *Nano Lett.* **2011**, *11*, 717 – 722.
[36] B. H. Son, J. K. Park, T. H. Jung, J. Y. Park, S. Lee, Y. H. Ahn, *ACS Nano* **2014**, *8*, 11361 – 11368.

Received: July 5, 2016
Published online: July 27, 2016

